

On chiral spin symmetry and the QCD phase diagram

Owe Philipsen,^{a,b,*} Leonid Ya. Glozman,^c Peter Lowdon^a and Robert D. Pisarski^d

^a*Institute for Theoretical Physics, Goethe University Frankfurt,
Max-von-Laue-Str. 1, D-60438 Frankfurt am Main, Germany*

^b*John von Neumann Institute for Computing (NIC)
at GSI, Planckstr. 1, 64291 Darmstadt, Germany*

^c*Institute of Physics, University of Graz, A-8010 Graz, Austria*

^d*Physics Department, Brookhaven National Laboratory, Upton, NY 11973, USA*

E-mail: philipsen@itp.uni-frankfurt.de

Recently, an approximate $SU(4)$ chiral spin-flavour symmetry was observed in multiplet patterns of QCD meson correlation functions, in a temperature range above the chiral crossover. This symmetry is larger than the chiral symmetry of massless QCD, and can only arise effectively when colour-electric quark-gluon interactions dynamically dominate the quantum effective action. At temperatures about three times the crossover temperature, these patterns disappear again, indicating the screening of colour-electric interactions, and the expected chiral symmetry is recovered. In this contribution we collect independent evidence for such an intermediate temperature range, based on screening masses and the pion spectral function. Both kinds of observables behave non-perturbatively in this window, with resonance-like peaks for the pion and its first excitation disappearing gradually with temperature. Using symmetry arguments and the known behaviour of screening masses at small densities, we discuss how this chiral spin symmetric band continues into the QCD phase diagram.

*The 39th International Symposium on Lattice Field Theory,
8th-13th August, 2022,
Rheinische Friedrich-Wilhelms-Universität Bonn, Bonn, Germany*

*Speaker

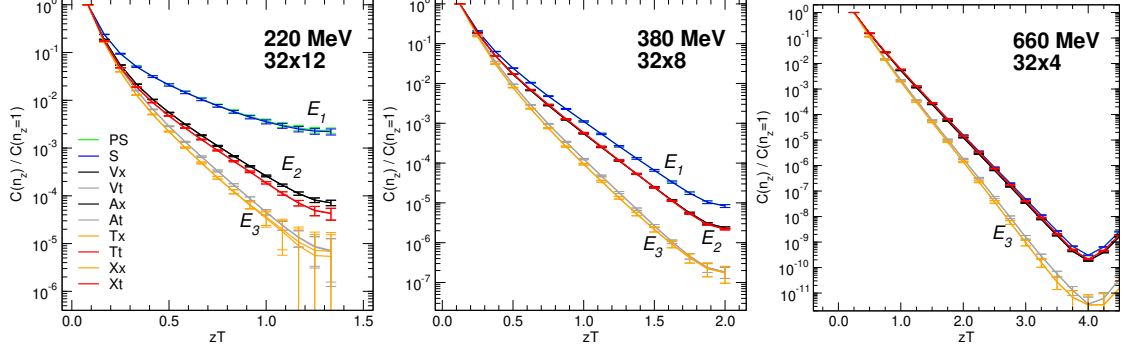


Figure 1: Spatial correlation functions show distinct E_1, E_2, E_3 multiplets of the approximate $SU(4)$ chiral symmetry, at temperatures above the crossover. At large temperatures, these reduce to the multiplets of the ordinary chiral symmetry. Based on domain wall fermions, from [4].

1. Introduction

While QCD at finite baryon density cannot be simulated by Monte Carlo methods because of a severe sign problem, the physics at finite temperature poses no technical complications and, given sufficient compute power, can be evaluated non-perturbatively. In particular, the nature of the chiral transition as an analytic crossover [1] and its associated pseudo-critical temperature T_{pc} [2, 3] are known with ever increasing precision.

However, the physics at temperatures above the chiral crossover appears to be different and more complex than expected so far. A few years ago an additional chiral spin symmetry was observed to emerge dynamically in a temperature range of roughly $T_{pc} \lesssim T \lesssim 3T_{pc}$ [4, 5]. This symmetry is larger than the chiral symmetry and can only be realised approximately if colour-electric quark-gluon interactions dominate the quantum effective action. This suggests that there are three temperature regimes in QCD with different effectively realised symmetries and dynamics. In this contribution we review the original evidence based on multiplets of spatial and temporal correlators [4, 5], and show that the associated change of dynamics is also visible in screening masses and the pion spectral function. We then discuss how this new band of effectively chiral spin symmetric QCD extends into the QCD phase diagram.

2. Emergent chiral spin symmetry at finite T

Consider a $SU(2)_{CS}$ chiral spin transformation of Dirac quark fields defined by

$$\psi(x) \rightarrow \exp\left(i\vec{\Sigma} \cdot \vec{\epsilon}\right)\psi(x), \quad \vec{\Sigma} = (\gamma_k, -i\gamma_5\gamma_k, \gamma_5), \quad [\Sigma_i, \Sigma_j] = 2i\epsilon_{ijk}\Sigma_k. \quad (1)$$

Here $k = 0, \dots, 3$ can be any of the euclidean gamma matrices, and it is easy to check that the generators $\vec{\Sigma}$ satisfy a $SU(2)$ algebra. It is apparent that $SU(2)_{CS} \supset U(1)_A$. Furthermore, when combined with isospin, $SU(2)_{CS} \otimes SU(2)_V$ can be embedded into the larger $SU(4)$, which contains the usual chiral symmetry of the massless QCD Lagrangian, $SU(4) \supset SU(2)_L \times SU(2)_R \times U(1)_A$.

The QCD Lagrangian is not invariant under chiral spin transformations. However, a thermal medium implies a preferred Lorentz frame, and the massless quark action can be written as

$$\bar{\psi}\gamma_\mu D_\mu\psi = \bar{\psi}\gamma_0 D_0\psi + \bar{\psi}\gamma_i D_i\psi, \quad \text{with} \quad [\Sigma_i, \gamma_0\gamma_0] = 0, \quad [\Sigma_i, \gamma_0\gamma_j] \neq 0. \quad (2)$$

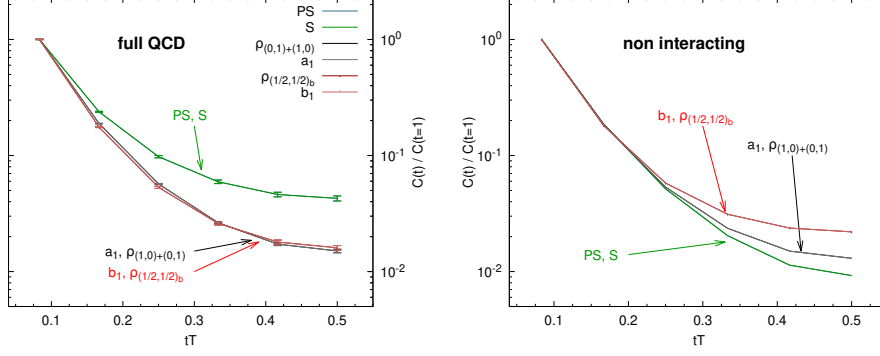


Figure 2: Temporal correlation functions on 12×48^3 lattices. Left: Full QCD results at $T = 220$ MeV, representing multiplets of all groups, $U(1)_A$, $SU(2)_L \times SU(2)_R$, $SU(2)_{CS}$ and $SU(4)$. Right: Correlators calculated with free quarks with manifest $U(1)_A$ and $SU(2)_L \times SU(2)_R$ symmetries. From [5].

One finds the colour-electric part of the quark-gluon interaction to be CS- and $SU(4)$ -invariant, while kinetic terms (and thus the free Dirac action) and colour-magnetic interactions are not. Hence, chiral spin symmetry is never exact in physical QCD, but its approximate realisation is possible if the colour-electric quark-gluon interaction dominates the quantum effective action in some dynamical range.

On the lattice, symmetries are straightforwardly tested by investigating degeneracy patterns in correlation functions. Consider the euclidean meson correlators with $J = 0, 1$ and Γ some appropriate Dirac matrix,

$$C_\Gamma(\tau, \mathbf{x}) = \langle O_\Gamma(\tau, \mathbf{x}) O_\Gamma^\dagger(0, \mathbf{0}) \rangle. \quad (3)$$

These carry the full information about all excitations in their associated spectral functions $\rho_\Gamma(\omega, \mathbf{p})$,

$$C_\Gamma(\tau, \mathbf{p}) = \int_0^\infty \frac{d\omega}{2\pi} K(\tau, \omega) \rho_\Gamma(\omega, \mathbf{p}), \quad K(\tau, \omega) = \frac{\cosh(\omega(\tau - 1/2T))}{\sinh(\omega/2T)}. \quad (4)$$

For an isotropic system in equilibrium, it is sufficient to probe the spatial and temporal correlators averaged over the orthogonal directions,

$$C_\Gamma^S(z) = \sum_{x,y,\tau} C_\Gamma(\tau, \mathbf{x}), \quad C_\Gamma^\tau(\tau) = \sum_{x,y,z} C_\Gamma(\tau, \mathbf{x}). \quad (5)$$

Numerical results obtained with $N_f = 2$ JLQCD domain wall fermions with good chiral symmetry and all lattice spacings < 0.1 fm [4, 5] are shown in Figs. 1 and 2, respectively. Fig. 1 shows three multiplets of spatial correlators, $E_{1,2,3}$, at different temperatures. Of these, E_1 is due to $U(1)_A$ restoration whereas E_3 requires the full chiral symmetry. Both multiplets are expected above the chiral crossover. What is surprising is the multiplet E_2 , which does *not* correspond to a representation of chiral symmetry, but to one of the larger $SU(4)$ (for the representations and their identification with meson states, see [6, 7]). Its distinctive appearance demonstrates the dynamical emergence of chiral spin symmetry in this regime. As temperature is further increased, E_2 gradually disappears as a separate multiplet and only those belonging to the expected chiral symmetry survive.

This finding is confirmed by the temporal correlators shown in Fig. 2 (left). In this case it is the degeneracy of the a_1 and b_1 correlators, which cannot be transformed into each other by ordinary

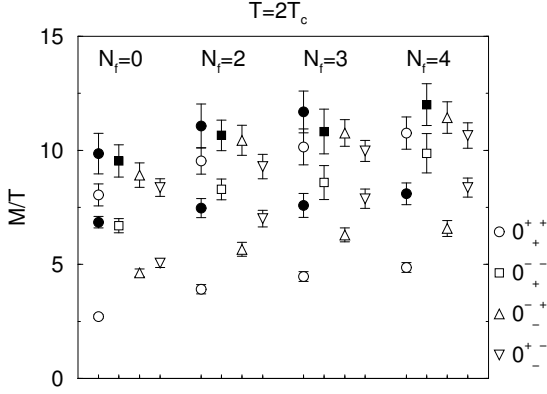


Figure 3: Screening masses computed within EQCD, after integrating out N_f massless fermions. Filled symbols correspond to operators constructed from colour-magnetic fields exclusively, $\text{Tr}F_{ij}^2, \dots$, open symbols contain colour-electric fields $\text{Tr}(A_0^2), \text{Tr}(A_0 F_{ij}), \dots$. From [8].

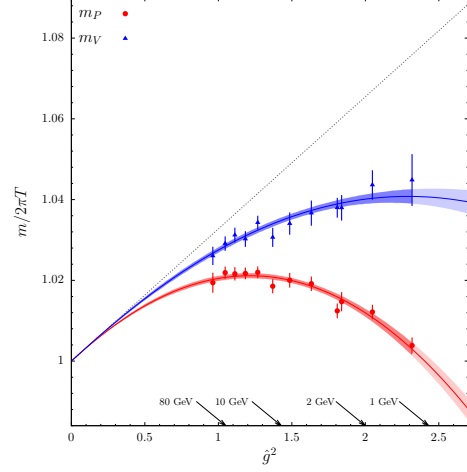


Figure 4: Pseudo-scalar and vector screening masses at high temperatures, based on $O(a)$ -improved Wilson fermions with modified boundary conditions and step scaling techniques. From [9].

chiral transformations, but are related via the larger $SU(4)$ symmetry. By contrast, Fig. 2 (right) shows the same correlators evaluated with free quarks, corresponding to the leading perturbative result, which respects the ordinary chiral symmetry. The degeneracy pattern and ordering are qualitatively incompatible with the QCD data.

One must then conclude that there are three temperature ranges with different symmetry properties: the regime of broken chiral symmetry at low temperatures, an approximately $SU(4)$ -symmetric regime for $T_{pc} \lesssim T \lesssim 3T_{pc}$, and the expected chirally symmetric regime at high temperatures. Usually changes in symmetry imply changes in dynamical behaviour and effective degrees of freedom. We now show that such changes are indeed visible also in other observables.

3. Screening masses

Although not directly measurable experimentally, QCD screening masses are valuable and well-studied observables, because they can be readily evaluated both non-perturbatively and perturbatively, permitting insights into the transition between the confined and deconfined regimes. They can be extracted from the exponential decay of spatial correlators,

$$C_{\Gamma}^S(z) \xrightarrow{z \rightarrow \infty} \text{const.} \cdot e^{-m_{scr} z}, \quad (6)$$

and correspond to the “zero momentum” eigenvalues of a “spatial Hamiltonian” H_z , which acts on states defined over $\{x, y, \tau\}$ -space and translates them in z direction,

$$|\psi(\tau, x, y; \cdot, z+1)\rangle = e^{-aH_z} |\psi(\tau, x, y; z)\rangle. \quad (7)$$

To begin, we recall evidence for the dynamical dominance of the colour-electric fields, which was produced in the context of dimensional reduction of finite temperature quantum field theories. It is well known that finite temperature gauge theories are characterised by three dynamical scales,

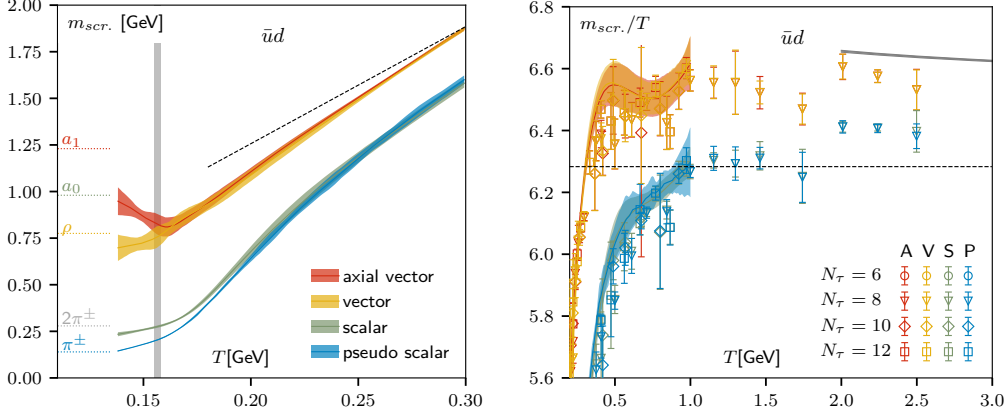


Figure 5: Screening masses of the lightest $\bar{u}d$ -mesons, evaluated using HISQ fermions. From [11].

the hard scale $\sim \pi T$ for the non-zero Matsubara/fermion modes, the soft scale $\sim gT$ for the colour-electric fields and the ultra-soft scale $\sim g^2 T$ for the entirely non-perturbative magnetic modes. In [8] EQCD, obtained as an effective bosonic theory after integrating out the hard modes perturbatively, was simulated and screening masses were computed for a range of quantum numbers, as shown in Fig. 3. One observes that, independent of the quantum number channel, the screening masses based on interpolating operators containing at least one A_0 field are considerably smaller than those constructed entirely from A_i -fields, which means the dynamics is dominated by colour-electric fields. This is reversed compared to the perturbative parametric ordering, and provides the necessary condition for an approximate realisation of chiral spin symmetry.

Next, we consider meson correlators in QCD, i.e. screening states living on the hard scale, which is the most likely to behave perturbatively. Recently, by employing shifted boundary conditions in combination with step scaling techniques on $N_f = 2$ $O(a)$ -improved Wilson fermions, it was possible to compute screening masses on the lattice in the high temperature regime, $T \sim 1 - 160$ GeV for the first time, with unprecedented precision [9]. Results for the pseudo-scalar and vector screening masses are shown in Fig. 4, the coloured bands represent fits of the data to the perturbative parametrisation

$$\frac{m_{PS}}{2\pi T} = 1 + p_2 \hat{g}^2(T) + p_3 \hat{g}^3(T) + p_4 \hat{g}^4(T), \quad \frac{m_V}{2\pi T} = \frac{m_{PS}}{2\pi T} + s_4 \hat{g}^4(T). \quad (8)$$

Here $\hat{g}^2(T)$ denotes the running coupling renormalised in the $\overline{\text{MS}}$ -scheme at $\mu = 2\pi T$, while $p_2 \dots p_4, s_4$ are numbers. The perturbative value of p_2 [10] is fully confirmed, as is the corresponding functional form Eq. (8), over a remarkable three orders of magnitude in temperature. The difference due to spin can be described by a single \hat{g}^4 -term.

Two dynamical changes, incompatible with perturbative behaviour, become apparent in the intermediate range $T \sim 0.15 - 1$ GeV, which was studied with $N_f = 2+1$ HISQ fermions at physical quark masses [11], as shown in Fig. 5. On the left one observes chiral symmetry restoration, with screening masses becoming degenerate at $T_{pc} \approx 150$ MeV, as expected (the degeneracy of the pion with the two-pion state instead of the a_0 is a known artefact of the staggered taste splitting [11, 12]). More interestingly, another marked change of dynamics is visible in the right plot, where m_{scr}/T changes from nearly vertical to almost horizontal behaviour within a narrow temperature range. At

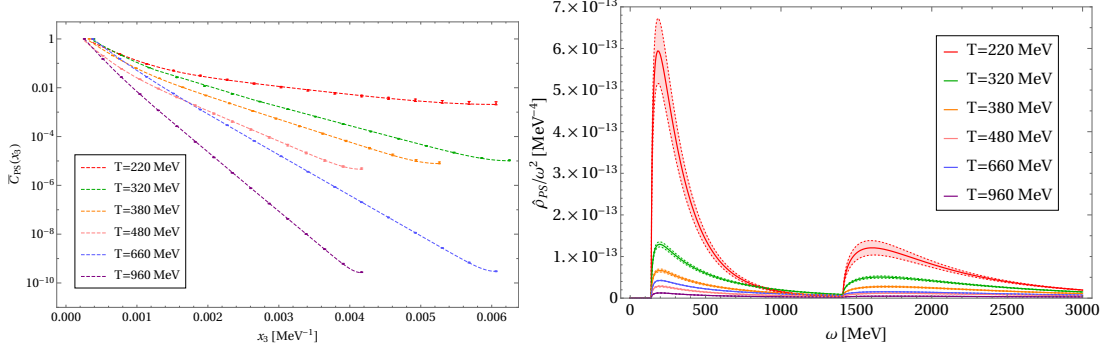


Figure 6: Left: Pseudo-scalar, spatial correlation functions from Fig. 1 [4], the lines represent two-state exponential fits. Right: Spectral function resulting from those fits and the ansatz Eqs. (10,11).

its high temperature end, the plot matches the behaviour from the previous figure, with all screening masses overshooting $\sim 2\pi T$ and a sizeable spin effect. Nevertheless (and ignoring the wiggles within errors), the horizontal part of the plot is fully compatible with Eq. (8) and its logarithmic T -dependence, i.e. perturbative behaviour. This changes abruptly between $T \sim 500 - 700$ MeV for all four quantum number channels shown in Fig. 5. The sudden change in T -dependence is not compatible with the perturbative behaviour Eq. (8), nor can it be accommodated by higher order corrections. The same abrupt bending is observed in the same T -range also for the $\bar{u}s$ and $\bar{s}s$ mesons [11], i.e. across 12 different quantum number channels, and therefore suggests a change of dynamics for the entire system. The temperature region, where this dynamical change happens, is fully compatible with the upper boundary of chiral spin symmetry, which explains the breakdown of perturbation theory: since the latter is organised around free quarks, it cannot accommodate chiral spin symmetry to any finite order. This breakdown of perturbation theory confirms the earlier conclusion based on symmetry alone, i.e. the presence of non-perturbative colour-electric interactions between quarks. For this reason this regime has been termed "stringy fluid" [4, 5].

4. The pion spectral function

More direct information about the nature of the effective degrees of freedom in the different regimes may be expected from the spectral functions, Eq. (4). Unfortunately, their extraction from discrete sets of lattice correlator data represents an ill-posed inversion problem. Here we try a new method that applies to stable scalar particles in a heat bath, i.e. to the pion in the case of QCD, which allows to circumvent the integral inversion.

The method is based on the fundamental principle of locality (in the sense of micro-causality) of quantum field theories. It ensures a representation of the spectral function [13, 14] as

$$\rho_{\text{PS}}(\omega, \mathbf{p}) = \int_0^\infty ds \int \frac{d^3 u}{(2\pi)^2} \epsilon(p_0) \delta(\omega^2 - (\mathbf{p} - \mathbf{u})^2 - s) \tilde{D}_\beta(\mathbf{u}, s), \quad (9)$$

with $\beta = 1/T$, the thermal spectral density $\tilde{D}_\beta(\mathbf{u}, s)$. Note that the standard Källen-Lehmann vacuum representation is attained smoothly as $T \rightarrow 0$. For stable massive particles, such as QCD pions, the authors argue for the analytic vacuum structure of the spectral density to be preserved in the

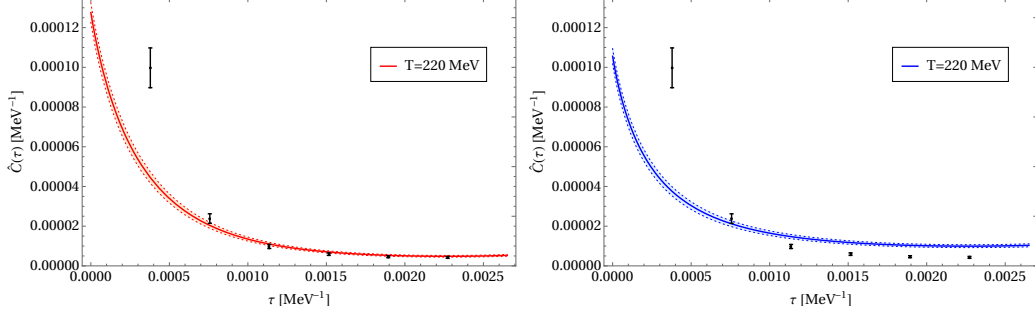


Figure 7: Left: Temporal correlation function predicted by the spectral function Eq. (12), Fig. 6 (red band), compared to the full lattice data from Fig. 2 [5]. Right: The corresponding prediction based on a Breit-Wigner ansatz, Eq. (13).

absence of a true phase transition, and propose an ansatz with particle and scattering contributions,

$$\tilde{D}_\beta(\mathbf{u}, s) = \tilde{D}_{m,\beta}(\mathbf{u}) \delta(s - m^2) + \tilde{D}_{c,\beta}(\mathbf{u}, s). \quad (10)$$

In an isotropic medium the spatial correlators and the spectral density are then related by [15]

$$C_{PS}^s(z) = \frac{1}{2} \int_0^\infty ds \int_{|z|}^\infty dR e^{-R\sqrt{s}} D_\beta(R, s). \quad (11)$$

For temperatures below the threshold to the scattering states we then expect the first term in Eq. (10) to dominate. Neglecting the continuum part, the calculation of the spectral function is straightforward. First, we fit the spatial pseudo-scalar correlators from Fig. 1 by the sum of two exponentials representing the π, π^* , which gives an excellent description of the data in the entire temperature range, cf. Fig. 6 (left). This provides the $D_{m,\beta}(|\mathbf{x}|) = \alpha_{\pi,\pi^*} \exp(-\gamma_{\pi,\pi^*} |\mathbf{x}|)$, from which the spectral function can be reconstructed using Eqs. (9,10) and the vacuum masses m_π, m_{π^*} ,

$$\rho_{PS}(\omega, \mathbf{p} = 0) = \epsilon(\omega) \left[\theta(\omega^2 - m_\pi^2) \frac{4 \alpha_\pi \gamma_\pi \sqrt{\omega^2 - m_\pi^2}}{(\omega^2 - m_\pi^2 + \gamma_\pi^2)^2} + \theta(\omega^2 - m_{\pi^*}^2) \frac{4 \alpha_{\pi^*} \gamma_{\pi^*} \sqrt{\omega^2 - m_{\pi^*}^2}}{(\omega^2 - m_{\pi^*}^2 + \gamma_{\pi^*}^2)^2} \right]. \quad (12)$$

The result is shown in Fig. 6 (right) and displays the vacuum thresholds followed by a pronounced resonance-like peak structure for both the pion and its first excitation. As the temperature increases, the peaks widen and gradually disappear into a continuum, consistent with sequential hadron melting, albeit at temperatures significantly above T_{pc} . This is in accord with the approximately chiral-spin symmetric window with non-perturbative, hadron-like excitations.

Since we neglected the continuum contribution from Eq. (10), it is crucial to perform a quality check. This is done in Fig. 7 (left), where we predict the temporal correlator C_{PS}^τ using our spectral function from the spatial correlator at $T = 220$ MeV, and compare with the lattice result from Fig. 2. Excellent quantitative agreement is found except for very short distances, which is due to the neglected higher excited states in the description of the spatial correlator. For higher temperatures we expect the quality of the prediction to deteriorate, as in this case the neglected continuum part $D_{c,\beta}$ should play an increasing role.

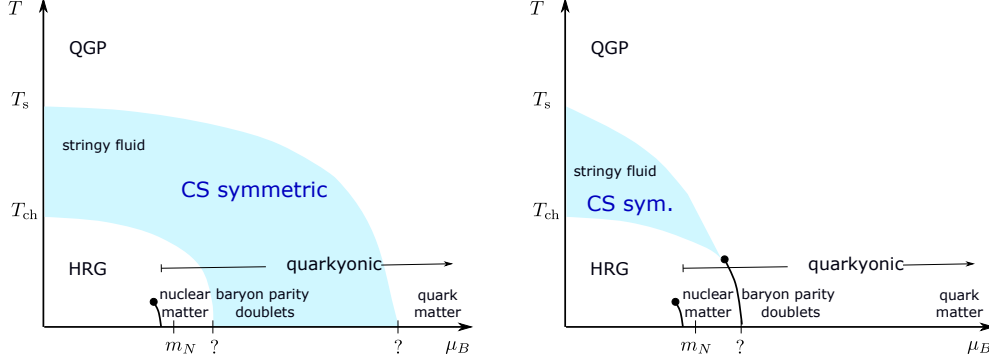


Figure 8: Possibilities for the QCD phase diagram with a chiral spin and $SU(4)$ -symmetric band.

For comparison, we have also tried a Breit-Wigner ansatz commonly associated with perturbative plasma excitations,

$$\rho_{PS}^{BW}(\omega, \mathbf{p} = 0) = \frac{4\alpha_\pi \omega \Gamma_\pi}{(\omega^2 - m_\pi^2 - \Gamma_\pi^2)^2 + 4\omega^2 \Gamma_\pi^2} + \frac{4\alpha_\pi^* \omega \Gamma_{\pi^*}}{(\omega^2 - m_{\pi^*}^2 - \Gamma_{\pi^*}^2)^2 + 4\omega^2 \Gamma_{\pi^*}^2}. \quad (13)$$

This ansatz can be fitted equally well to the spatial correlator at $T = 220$ MeV, but in this case the predicted temporal correlator is not compatible with the data, Fig. 7 (right).

5. The QCD phase diagram

Having established an effectively chiral spin symmetric temperature window at zero density with non-perturbative dynamics, the question is what happens at finite baryon chemical potential. This adds $\mu_B/3 \bar{\psi} \gamma_0 \psi$ to the effective Lagrangian, and since the generators of chiral spin commute with γ_0 , Eq. (2), an approximate chiral spin symmetry at zero density must continue to $\mu_B \neq 0$. At least for $\mu_B/T \lesssim 3$ we can then infer what happens to the chiral spin symmetric band.

Since full chiral symmetry restoration is necessary for chiral spin symmetry, its lower boundary $T_{ch}(\mu) \gtrsim T_{pc}(\mu)$. In Sec. 3 we identified the upper crossover T_s by the bending of the screening masses, which marks the screening of the colour-electric interactions and the onset of perturbative behaviour. Picking the vector meson screening radius at its bend to define the screening temperature T_s ,

$$r_V^{-1}(\mu_B = 0, T_s) \equiv m_V(\mu_B = 0, T_s) = C_0 T_s, \quad (14)$$

we can use the Taylor expanded screening mass to deduce the line of constant r_V^{-1} ,

$$\frac{m_V(\mu_B)}{T} = C_0 + C_2 \left(\frac{\mu_B}{T}\right)^2 + \dots \Rightarrow \frac{dT_s}{d\mu_B} = -\frac{2C_2 \mu_B}{C_0 T} - \frac{2C_2^2}{C_0^2} \left(\frac{\mu_B}{T}\right)^3 + \dots \quad (15)$$

Since $C_2 > 0$ [16, 17], the upper crossover line bends downwards, as indicated in Fig. 8.

As chemical potential increases, further details of the phase diagram remain unknown, and several options for the continuation of the chiral spin symmetric band are possible. In the cold and dense regime, baryon parity doublet matter is consistent with chiral spin symmetry, provided it is decoupled from π, σ to leading order, otherwise it is only chirally symmetric. Similarly, quarkyonic matter with a chirally symmetric confined regime [18, 19] may also be chiral spin symmetric, as discussed in [20]. This is independent of the question whether or not there is a non-analytic chiral phase transition. Two possibilities (there are more) for the phase diagram are shown in Fig. 8.

6. Conclusions and outlook

For QCD at the physical point at zero density, there appear to exist three temperature regimes with different effective symmetries, separated by two crossovers. The low temperature hadronic regime with broken chiral symmetry is, somewhere above the chiral crossover T_{pc} , followed by a regime with an approximate $SU(4)$ symmetry, which features non-perturbative dynamics as shown by screening masses, and resonance-like pion states. This is consistent with a dominant colour-electric quark-gluon interaction, as suggested by the effective symmetry. At a second crossover around $\sim 3T_{pc}$, the symmetry is reduced to the expected chiral symmetry, screening masses follow perturbative behaviour and the resonance-like pion peaks have disappeared. We have argued by symmetry and the known behaviour of screening masses, that this chiral spin symmetric band should continue to finite baryon density and bend downwards, with several possibilities for the QCD phase diagram.

There is now an entire range of feasible lattice projects to clarify the range and properties of the chiral spin symmetric band. In particular, the pseudo-critical $T_s(\mu)$ can be mapped out just as far as $T_{pc}(\mu)$, using lattice methods such as imaginary chemical potential, Taylor expansion or reweighting. To obtain further insight into the dynamics, spectral functions should be studied in other quantum number channels as well. To this end, we have demonstrated that much tighter constraints are obtained once both spatial *and* temporal correlators are available with good precision.

Acknowledgments

O.P. and P.L. acknowledge support by the Deutsche Forschungsgemeinschaft (DFG) through the grant CRC-TR 211 “Strong-interaction matter under extreme conditions”. O.P. further acknowledges support by the State of Hesse within the Research Cluster ELEMENTS (Project ID 500/10.006).

References

- [1] Y. Aoki, G. Endrodi, Z. Fodor, S.D. Katz and K.K. Szabo, *The Order of the quantum chromodynamics transition predicted by the standard model of particle physics*, *Nature* **443** (2006) 675 [[hep-lat/0611014](#)].
- [2] HotQCD collaboration, *Chiral crossover in QCD at zero and non-zero chemical potentials*, *Phys. Lett. B* **795** (2019) 15 [[1812.08235](#)].
- [3] S. Borsanyi, Z. Fodor, J.N. Guenther, R. Kara, S.D. Katz, P. Parotto et al., *QCD Crossover at Finite Chemical Potential from Lattice Simulations*, *Phys. Rev. Lett.* **125** (2020) 052001 [[2002.02821](#)].
- [4] C. Rohrhofer, Y. Aoki, G. Cossu, H. Fukaya, C. Gattringer, L.Y. Glozman et al., *Symmetries of spatial meson correlators in high temperature QCD*, *Phys. Rev. D* **100** (2019) 014502 [[1902.03191](#)].
- [5] C. Rohrhofer, Y. Aoki, L.Y. Glozman and S. Hashimoto, *Chiral-spin symmetry of the meson spectral function above T_c* , *Phys. Lett. B* **802** (2020) 135245 [[1909.00927](#)].

- [6] L.Y. Glozman, *SU(4) symmetry of the dynamical QCD string and genesis of hadron spectra*, *Eur. Phys. J. A* **51** (2015) 27 [1407.2798].
- [7] L.Y. Glozman and M. Pak, *Exploring a new SU(4) symmetry of meson interpolators*, *Phys. Rev. D* **92** (2015) 016001 [1504.02323].
- [8] A. Hart, M. Laine and O. Philipsen, *Static correlation lengths in QCD at high temperatures and finite densities*, *Nucl. Phys. B* **586** (2000) 443 [hep-ph/0004060].
- [9] M. Dalla Brida, L. Giusti, T. Harris, D. Laudicina and M. Pepe, *Non-perturbative thermal QCD at all temperatures: the case of mesonic screening masses*, *JHEP* **04** (2022) 034 [2112.05427].
- [10] M. Laine and M. Vepsalainen, *Mesonic correlation lengths in high temperature QCD*, *JHEP* **02** (2004) 004 [hep-ph/0311268].
- [11] A. Bazavov et al., *Meson screening masses in (2+1)-flavor QCD*, *Phys. Rev. D* **100** (2019) 094510 [1908.09552].
- [12] S. Prelovsek, *Effects of staggered fermions and mixed actions on the scalar correlator*, *Phys. Rev. D* **73** (2006) 014506 [hep-lat/0510080].
- [13] J. Bros and D. Buchholz, *Towards a relativistic KMS condition*, *Nucl. Phys. B* **429** (1994) 291 [hep-th/9807099].
- [14] J. Bros and D. Buchholz, *Axiomatic analyticity properties and representations of particles in thermal quantum field theory*, *Ann. Inst. H. Poincaré Phys. Théor.* **64** (1996) 495 [hep-th/9606046].
- [15] P. Lowdon and O. Philipsen, *Pion spectral properties above the chiral crossover of QCD*, *JHEP* **10** (2022) 161 [2207.14718].
- [16] A. Hart, M. Laine and O. Philipsen, *Testing imaginary versus real chemical potential in finite temperature QCD*, *Phys. Lett. B* **505** (2001) 141 [hep-lat/0010008].
- [17] QCD-TARO collaboration, *Properties of hadron screening masses at finite baryonic density*, *Phys. Lett. B* **609** (2005) 265 [hep-lat/0410017].
- [18] L. McLerran and R.D. Pisarski, *Phases of cold, dense quarks at large N_c* , *Nucl. Phys. A* **796** (2007) 83 [0706.2191].
- [19] O. Philipsen and J. Scheunert, *QCD in the heavy dense regime for general N_c : on the existence of quarkyonic matter*, *JHEP* **11** (2019) 022 [1908.03136].
- [20] L.Y. Glozman, O. Philipsen and R.D. Pisarski, *Chiral spin symmetry and the QCD phase diagram*, 2204.05083.